Straining of colloids at textural interfaces

Scott A. Bradford,[1] Jirka Simunek,[2] Mehdi Bettahar,[3] Yadata F. Tadassa,[1]
Martinus T. van Genuchten,[1] and Scott R. Yates[1]

Received 22 September 2004; revised 22 April 2005; accepted 23 June 2005; published 11 October 2005.

[1] Although natural soil and aquifer systems often contain layers and lenses of contrasting soil texture, relatively little research has focused on the mechanisms of colloid deposition at textural interfaces. Saturated column studies were undertaken to characterize the straining behavior of negatively charged latex colloids (1.1 and 3.0 μm) at textural interfaces. Mechanisms of colloid transport and retention were deduced from measured effluent concentration curves, final spatial distributions in the columns, mass balance information, microscopic examination of deposition behavior in micromodel experiments, and numerical modeling. Transport and deposition of colloids were found to be highly dependent upon the textural interface. Deposition of colloids in a given sand was always most pronounced at the sand (inlet) surface. Here colloids enter a new pore network and are more likely to encounter smaller pores or dead-end regions of the pore space that contribute to straining. Less deposition occurred at textural interfaces within the column than at the sand surface. We believe that this is due to the fact that advection, dispersion, and size exclusion tend to confine colloid transport to the larger pore networks, thus limiting accessibility to straining sites. Increasing the textural contrast at an interface produced greater colloid deposition when water flowed from coarser- to finer-textured sands. Conversely, when water flowed from finer- to coarser-textured sands, little deposition occurred. Numerical modeling indicates the need to account for blocking (filling) and accessibility of straining sites in layered systems. A previously developed straining model was modified to account for this behavior.

Citation: Bradford, S. A., J. Simunek, M. Bettahar, Y. F. Tadassa, M. T. van Genuchten, and S. R. Yates (2005), Straining of colloids at textural interfaces, *Water Resour. Res.*, *41*, W10404, doi:10.1029/2004WR003675.

1. Introduction

[2] Considerable research has been devoted to the transport and fate of colloids in porous media [*Schijven and Hassanizadeh*, 2000; *Harvey and Harms*, 2002; *Jin and Flury*, 2002; *Ginn et al.*, 2002; *de Jonge et al.*, 2004; *McCarthy and McKay*, 2004; *DeNovio et al.*, 2004]. Knowledge of mechanisms that control colloid migration is required to protect drinking water supplies from pathogenic microorganisms [*Bitton and Harvey*, 1992], to develop engineered bioaugmentation and bioremediation strategies [*Wilson et al.*, 1986; *Rockhold et al.*, 2004], and to devise microbially enhanced oil recovery systems [*MacLeod et al.*, 1988]. The environmental fate of many organic and inorganic contaminants can also be influenced by colloid-facilitated transport due to partitioning onto high surface area colloids that are mobile [*Kretzschmar et al.*, 1999; *Ouyang et al.*, 1996; *de Jonge et al.*, 2004].

[3] Attachment (adsorption) is a mechanism for colloid retention that involves collision with and fixation to the porous medium. Attachment depends on colloid-colloid, colloid-solvent, and colloid-porous media interactions [*Elimelech and O'Melia*, 1990]. Clean bed attachment behavior is traditionally described as a first-order process, which implies that retained colloids will be distributed in an exponential manner versus distance. Attachment theory predicts an optimum size for colloid transport in a given porous medium, with diffusion controlling the transport of smaller particles, and sedimentation and interception the transport of larger colloids [*Logan et al.*, 1995].

[4] Experimental effluent concentration curves and spatial distributions of retained colloids in porous media have not always been in agreement with colloid attachment theory [*Camesano and Logan*, 1998; *Bolster et al.*, 1999; *Redman et al.*, 2001; *Bradford et al.*, 2002; *Tufenkji et al.*, 2003; *Li et al.*, 2004; *Tufenkji and Elimelech*, 2005]. Some of these discrepancies have been attributed to soil surface roughness [*Redman et al.*, 2001; *Kretzschmar et al.*, 1997] and charge variability [*Johnson and Elimelech*, 1995], heterogeneity in colloid characteristics [*Bolster et al.*, 1999; *Li et al.*, 2004], colloid detachment [*Tufenkji et al.*, 2003], time-dependent attachment behavior [*Johnson and Elimelech*, 1995], deposition of colloids in a secondary energy minimum [*Redman et al.*, 2004; *Tufenkji and Elimelech*, 2005], and straining [*Bradford et al.*, 2002, 2003, 2004; *Li et al.*, 2004; *Tufenkji et al.*, 2004; *Bradford and Bettahar*, 2005; *Foppen et al.*, 2005].

[5] Straining involves the entrapment of colloids in down gradient pores and at grain junctions that are too small to allow particle passage. The critical pore size for straining

[1] George E. Brown, Jr., Salinity Laboratory, ARS, USDA, Riverside, California, USA.
[2] Department of Environmental Sciences, University of California, Riverside, California, USA.
[3] Parsons, Pasadena, California, USA.

0043-1397/05/2004WR003675$09.00

will depend on the size of the colloid and the pore size distribution of the medium [*McDowell-Boyer et al.*, 1986; *Bradford et al.*, 2002, 2003]. *Matthess and Pekdeger* [1985] presented theoretical criteria suggesting that the ratio of the colloid (d_c) to median grain diameter (d_{50}) needs to be greater than 0.18 for straining to occur in uniform sand; increasing sand gradation would somewhat lower this threshold. For this reason most previous studies on colloid transport have neglected straining as a mechanism for retention [cf. *Schijven and Hassanizadeh*, 2000; *Harvey and Harms*, 2002; *Jin and Flury*, 2002; *Ginn et al.*, 2002]. Experimental observations, however, suggest that straining may occur for much lower values of d_c/d_{50}. *Sakthivadivel* [1966, 1969] reported that straining produced a permeability reduction of between 10 and 50% when d_c/d_{50} was around 0.05. *Bradford et al.* [2002, 2003] observed systematic trends of lower effluent concentrations and increasing colloid retention in sand near the column inlet with decreasing sand grain size or increasing colloid size. Mathematical modeling indicated that straining already occurred for $d_c/d_{50} > 0.005$. Data from *Li et al.* [2004] indicates that straining may have occurred for $d_c/d_{50} = 0.002$, but decreased with increasing pore water velocity. Results from *Tufenkji et al.* [2004] suggest that irregularity of the sand grain shape significantly contributes to the straining potential of porous media. *Foppen et al.* [2005] found that the rate of filling of straining sites was dependent on the concentration of colloids (bacteria) in suspension.

[6] Measured capillary pressure curves and residual saturations can be related to pore size distributions according to Laplace's equation of capillarity. The percentage of pore space where straining and size exclusion occurs can be inferred from this pore size distribution information. *Carsel and Parrish* [1988] present average capillary pressure curve parameters for the 12 major soil textural groups. Depending on soil texture, straining is predicted in 10.5 to 70.8% of the soil pore space for 0.1 μm size colloids; larger colloids produce even greater percentages. Conversely, mobile colloids that are not strained may be physically excluded (size exclusion) from this same fraction of the pore space.

[7] Size exclusion affects the mobility of colloids by constraining them to more conductive flow domains and larger pore networks that are physically accessible [*Ryan and Elimelech*, 1996; *Ginn*, 2002]. As a result, colloids can be transported faster than a conservative solute tracer [*Reimus*, 1995; *Cumbie and McKay*, 1999; *Harter et al.*, 2000; *Bradford et al.*, 2003]. Differences in the dispersive flux for colloids and a conservative solute tracer are also anticipated as a result of size exclusion [*Scheibe and Wood*, 2003]. *Bradford et al.* [2002] observed that the dispersivity of 3.2 μm carboxyl latex colloids was up to 7 times greater than bromide in saturated aquifer sand. Conversely, *Sinton et al.* [2000] found in a field microbial transport experiment that the apparent colloid dispersivity decreased with increasing particle size.

[8] Straining and size exclusion have significant implications for colloid transport in the field. Increased straining near the column inlet is deemed especially noteworthy since it may have ramifications for layered soil profiles, heterogeneous subsurface formations, artificially constructed media such as landfills, and water treatment techniques that are based on soil passage (riverbank filtration, infiltration basins and trenches, and sand filters). Much of the transport of colloids will then occur in the "hydraulically" active network of the larger pores. We postulate that straining is most pronounced at the soil surface or at the boundary of different soil textures where colloids are encountering a (new) pore network. At such boundaries, colloids are more likely to encounter a pore smaller than the critical straining size or one larger than the critical size that steers colloids toward "dead-end regions" of the pore space. Once colloids have entered the hydraulically active network, transport processes such as advection, dispersion, and size exclusion make it more likely for the colloids to remain confined to the network.

[9] Although natural soil and aquifer systems often contain layers and lenses of contrasting soil texture, relatively little research attention has focused on the mechanisms of colloid retention at textural interfaces [*Saiers et al.*, 1994; *Silliman*, 1995; *Bradford et al.*, 2004]. *Saiers et al.* [1994] found that colloid transport and deposition could be adequately described with an advection-dispersion transport model that accounted for first-order kinetic attachment/detachment. In contrast, *Silliman* [1995] found significant colloid retention at textural interfaces where water moved from larger to smaller diameter sands. This observation was attributed to straining initiated by colloid attachment. *Bradford et al.* [2004] found that colloid transport in heterogeneous systems was controlled primarily by straining when $d_c/d_{50} > 0.005$, but that attachment and the aqueous phase flow field (flow bypassing) also played important roles.

[10] The objective of this work is to investigate the main processes controlling the transport and fate of colloids across textural interfaces. While such information is needed to accurately assess colloid transport in heterogeneous aquifer formations, few studies have thus far systematically focused on this topic. It seems logical to anticipate that straining will be most pronounced at locations where colloids encounter a new pore network (e.g., textural interfaces). Colloid transport experiments were conducted using homogeneous and layered sand systems (using both columns and micromodels). Transport and retention were assessed by measuring temporal changes in colloid effluent concentrations and by studying the final spatial distribution of colloids remaining in the sand columns, as well as by microscopically studying locations of colloid deposition in homogeneous and layered sand experiments conducted in a glass micromodel (0.2 cm × 2.0 cm × 7.0 cm). The column transport data were described and analyzed using a transport model that accounts for advective, dispersive, and diffusive colloid fluxes, and two-site kinetic deposition. One deposition site is used to account for conventional first-order attachment and detachment, while the second deposition site includes a formulation for accessibility straining sites.

2. Materials and Methods

2.1. Colloids

[11] Yellow-green fluorescent latex microspheres (Interfacial Dynamics Company, Portland, OR) were used as model colloid particles in the experimental studies (excitation at 490 nm, and emission at 515 nm). Two sizes of microspheres were used in the transport experiments, 1.1

and 3.0 μm. The uniformity of the colloid size distributions was verified using with a Horiba LA 930 (Horiba Instruments Inc., Irvine, California) laser scattering particle size and distribution analyzer. These microspheres had sulfate surface functional groups, a density of 1.055 g cm^{-3} (provided by the manufacturer), and an equilibrium contact angle (air-water-lawn of colloids) of 101° (measured with a Tantec Contact Angle Meter, Tantec Inc., Schaumburg, Illinois). The 1.1 and 3.0 μm colloids had a surface charge density of 5.2 and 14.3 μC cm^{-2} (provided by manufacturer) and a zeta potential of −66.5 and −75.5 mV (measured with a ZetaPALs Instrument), respectively. The initial influent concentration (C_i) for the 1.1 and 3.0 μm colloids for the experiments was 3.3×10^{10} and 1.5×10^{9} N_c L^{-1} (where N_c denotes number of colloids), respectively. One experiment was conducted using 1.1 μm particles at $0.5^*C_i = 1.65 \times 10^{10}$ N_c L^{-1}.

2.2. Sand

[12] Aquifer material used for the column experiments consisted of various sieve sizes of Ottawa (quartz) sand (U.S. Silica, Ottawa, IL). The porous media were selected to encompass a range in grain sizes, and are designated by their median grain size (d_{50}) as: 710, 360, 240, and 150 μm. Specific properties of the 710, 360, 240, and 150 μm sands include: the coefficient of uniformity (d_{60}/d_{10}; here x% of the mass is finer than d_x) of 1.21, 1.88, 3.06, and 2.25; and intrinsic permeabilities of 4.08×10^{-10}, 6.37×10^{-11}, 1.12×10^{-11}, and 4.68×10^{-12} m^2, respectively. Ottawa sands typically consist of 99.8% SiO_2 (quartz) and trace amounts of metal oxides, have spheroidal shapes, and contain relatively rough surfaces. The vast majority of the sands possess a net negative charge at a neutral pH.

[13] *Bradford and Abriola* [2001] presented capillary pressure–saturation curves for the 710, 360, 240, and 150 μm sands. An estimate of the pore size distribution of drained pores (that may produce straining) can be obtained from capillary pressure–saturation curves using Laplace's equation of capillarity. Unfortunately, it is relatively difficult to use this method to characterize the small pore sizes of sands because of the presence of residual water (due to discontinuities in the wetting films). Alternatively, *Herzig et al.* [1970] calculated the volume of spherical colloids that could be retained in pores based on geometric considerations. The percentage of the total column volume retained by straining was calculated (assuming a coordination number of 7, a porosity of 0.35, a colloid diameter of 1.1 μm, and a grain diameter equal to d_{10}) to be 0.0002% for the 710 μm sands, 0.0020% for the 360 μm sands, 0.0129% for the 240 μm sands, and 0.0225% for the 150 μm sands. Although these straining volumes are quite small, significant numbers of colloids are required to fill the sites [*Foppen et al.*, 2005]. For example, 6.3×10^{10} colloids (1.1 μm) would be required to fully saturate (fill) all the straining sites in uniform 150 μm sand packed in a column that is 10 cm long and has an inside diameter of 5 cm. This corresponds to complete retention of 1.1 μm colloids in 27.9 pore volumes (PV) of suspension at a concentration of 3.3×10^{10} N_c L^{-1}.

2.3. Aqueous Phase

[14] The aqueous phase chemistry (pH, ionic strength, and composition) of the experimental solutions utilized in the column studies consisted of deionized water with its pH buffered to 6.98 using 5×10^{-5} M $NaHCO_3$ (ionic strength equal to 5×10^{-5} M). This solution was chosen to create a stabilized monodispersed suspension with the selected colloids, and to minimize electrostatic interactions between the colloids and porous media (highly unfavorable attachment conditions). The colloid tracer solution consisted of this same solution but with the previously indicated initial colloid concentration.

2.4. Column Experiments

[15] Procedures and protocols for the packed column experiments were previously discussed in detail by *Bradford et al.* [2002]. Only an abbreviated discussion is provided below. Kontes Chromaflex chromatography columns (Kimble/Kontes, Vineland, New Jersey) made of borosilicate glass (15 cm long and 4.8 inside diameter were equipped with an adjustable adapter at the top) were used in the transport studies. The columns were wet packed (water level kept above the sand surface) with the various porous media. For the layered experiments, equal mass fractions of the two sand types were successively packed into a column, taking care to minimize the disturbance at the textural interface. Table 1 provides porosity (ε) values [*Danielson and Sutherland*, 1986] and column length (L_c) for each experimental system. The colloid suspension was pumped upward through the vertically oriented columns at a steady flow rate for 77.5 (for C_i experiments) or 150 (0.5^*C_i experiment) min, after which a three-way valve was used to switch to the background solution for a total experimental time of 250 min. The average Darcian flux densities (q) for the various experiments are given in Table 1. Effluent samples were collected and analyzed for colloid concentration using a Turner Quantech fluorometer (Barnstead/Thermolyne, Dubuque, Iowa). The average of three measurements were used to determine each colloid concentration (reproducibility was typically within 1% of C_i).

[16] Following completion of the colloid transport experiments, the spatial distributions of colloids in the packed columns were determined. The saturated sand was carefully excavated into 50 mL Falcon centrifuge tubes containing excess deionized water. The tubes were slowly shaken for 15 min using a Eberbach shaker (Eberbach Corporation, Ann Arbor, Michigan) to liberate retained colloids. The concentration of the colloids in the excess aqueous solution was measured with a Turner Quantech fluorometer using the same experimental protocol as followed for the effluent samples. These concentrations were corrected for colloid release efficiency determined from batch experiments. The release efficiencies for 1.1 μm colloids were 0.78 in the 710 μm sand, 0.75 in the 360 μm sand, 0.71 in the 240 μm sand, and 0.68 in the 150 μm sand, while the 3.0 μm colloids had release efficiencies of 0.80 in the 710 μm sand and 0.78 in the 150 μm sand.

[17] A colloid mass balance was conducted at the end of each column experiment using effluent concentration data and the final spatial distribution of retained colloids in the sands. The calculated number of effluent and colloids retained in the sand was normalized by the total number of injected particles into a column. Table 1 presents the calculated effluent (M_e), sand (M_s), and the total ($M_t = M_e + M_s$) colloid mass fractions recovered for the various experiments.

Table 1. Packed Column Properties (Porosity, ε, Darcy Water Velocity, q, and Column Length, L_c) and the Recovered Effluent (M_e), Sand (M_s), and the Total Colloid Mass Fraction (M_t)

System	d_c, μm	ε	q, cm min^{-1}	L_c, cm	M_e	M_s	M_t
710	1.1	0.350	0.094	12.8	0.775	0.079	0.854
710	3.0	0.348	0.096	12.8	0.782	0.124	0.906
360	1.1	0.333	0.108	12.5	0.641	0.247	0.888
240	1.1	0.309	0.117	12.1	0.534	0.369	0.903
150	1.1	0.338	0.105	12.6	0.566	0.434	1.000
150[a]	1.1	0.345	0.106	12.7	0.572	0.463	1.035
150	3.0	0.344	0.103	12.7	0.039	0.978	1.017
150/710	1.1	0.335	0.113	12.5	0.650	0.359	1.009
150/710	3.0	0.356	0.116	13.0	0.062	0.530	0.592
150/360	1.1	0.342	0.123	12.7	0.622	0.320	0.942
150/240	1.1	0.326	0.133	12.4	0.549	0.433	0.982
710/360	1.1	0.345	0.085	12.7	0.703	0.233	0.936
710/240	1.1	0.345	0.097	12.7	0.669	0.270	0.939
710/150	1.1	0.353	0.101	12.9	0.676	0.286	0.962
710/150	3.0	0.356	0.098	13.0	0.384	0.634	1.018
360/240	1.1	0.323	0.108	12.3	0.485	0.594	1.079
360/150	1.1	0.327	0.102	12.4	0.516	0.568	1.084
240/150	1.1	0.328	0.092	12.4	0.386	0.679	1.065

[a]Input concentration equal to 0.5 C_i.

2.5. Micromodel Experiments

[18] Several transport experiments were conducted in a specially designed micromodel to examine the deposition behavior of the 1.1 and 3.0 μm sulfate colloids in homogeneous (150 μm sand) and layered (710/150) sand systems. The micromodel consisted of a 0.2 cm thick by 2.0 cm wide by 7 cm long glass chamber (inside dimensions), with a glass tube (0.5 cm inside diameter) and septum assembly joined at both ends of the chamber. The tubing was connected to the chamber by a glass blower at an angle of about 45°, so that the micromodel could lay flat on a horizontal surface. During packing the micromodel chamber was oriented vertically without the top septum. The desired sands were then wet packed in the chamber (homogeneous or layered configurations). Hypodermic needles and Teflon tubing were used to connect the inlet side of the chamber to a LabAlliance chromatography pump (State College, Pennsylvania) and a reservoir on the outlet side of the chamber. To be comparable to the column experiments, the colloid suspension was pumped at a steady rate of 0.04 ml min^{-1} (Darcy velocity of 0.1 cm min^{-1}) for about 60 min (around 2.5 pore volumes), followed by deionized water for an additional 60 min. After completion of a transport experiment, the hypodermic needles were removed and the final deposition behavior of the fluorescent colloids was microscopically examined at several locations using a Leica DM IRB epifluorescent microscope (Leica Microsystems Inc., Bannockburn, Illinois). Images were captured by connecting the microscope to a video monitor and computer system. Photographs (600 times magnification) were taken using various intensities of both UV and visible light so that sand grains and fluorescent colloids could be visualized simultaneously.

2.6. Theory and Model

[19] The aqueous phase colloid mass balance equation is written as

$$\frac{\partial(\theta_w C)}{\partial t} = -\nabla \cdot J_T - E_{sw}^{att} - E_{sw}^{str} \quad (1)$$

where C [N_c L^{-3}] is the colloid concentration in the aqueous phase, t [T] is time, θ_w (dimensionless) is the volumetric water content, J_T [N$_c$ L^{-2} T^{-1}] is the total colloid flux (sum of the advective, dispersive, and diffusive fluxes), and E_{sw}^{att} [N$_c$ L^{-3} T^{-1}] and E_{sw}^{str} [N$_c$ L^{-3} T^{-1}] are the colloid mass transfer terms between the aqueous and solid phases due to colloid attachment/detachment and straining, respectively. An expression for E_{sw}^{att} can be written as

$$E_{sw}^{att} = \rho_b \frac{\partial(S_{att})}{\partial t} = \theta_w k_{att} \psi_{att} C - \rho_b k_{\mathrm{det}} S_{att} \quad (2)$$

Here ρ_b [M L^{-3}] is the soil bulk density, S_{att} [N$_c$ M^{-1}] is the solid phase concentration of attached colloids, ψ_{att} (dimensionless) is a dimensionless colloid attachment function, and k_{att} [T^{-1}] and k_{det} [T^{-1}] are the first-order colloid attachment and detachment coefficients, respectively. When $\psi_{att} = 1$ and $k_{det} = 0$, clean bed attachment is assumed (leading to an exponential spatial distribution), while traditional filtration theory [*Logan et al.*, 1995] can be used as needed for k_{att} [e.g., *Bradford et al.*, 2003]. In contrast, to account for colloid blocking (filling of favorable attachment sites) the value of ψ_{att} decreases with increasing S_{att}. According to the Langmuirian approach [e.g., *Deshpande and Shonnard*, 1999], $\psi_{att} = 1 - S_{att}/S_{att}^{\max}$; where $S_{att}^{\max}$ [N$_c$ M^{-1}] is the maximum solid phase concentration of attached colloids. For given values of k_{att} and k_{det}, a decreasing $S_{att}^{\max}$ tends to produce higher effluent concentrations and lower values of S_{att}.

[20] Straining is modeled according to a slightly modified form of the approach described by *Bradford et al.* [2003]. The mass balance equation for strained colloids is given as

$$E_{sw}^{str} = \rho_b \frac{\partial(S_{str})}{\partial t} = \theta_w k_{str} \psi_{str} C \quad (3)$$

where k_{str} [T^{-1}] is the straining coefficient, ψ_{str} (dimensionless) is a dimensionless colloid straining function, and S_{str} [N$_c$ M^{-1}] is the solid phase concentration of strained colloids. The value of ψ_{str} for each layer is a function of distance and described as

$$\psi_{str} = H(z - z_o)\left(1 - \frac{S_{str}}{S_{str}^{\max}}\right)\left(\frac{d_{50} + z - z_o}{d_{50}}\right)^{-\beta} \quad (4)$$

where $H(z - z_o)$ is the Heaviside function, z [L] is depth, z_o [L] denotes the depth of the column inlet or textural interface, $S_{str}^{\max}$ [N$_c$ M^{-1}] is the maximum solid phase concentration of strained colloids, and β (dimensionless) is a parameter that controls the shape of the colloid spatial distribution. The Heaviside function is equal to 0 for $z < z_o$ and 1 for z greater than or equal to z_o. In homogeneous systems, the value of z_o equals the z coordinate of the sand surface. In layered systems, the value of z_o equals the z coordinate of the sand surface for the first layer, and the z coordinate of the interface for the second layer.

[21] The second term on the right hand side of equation (4) is included to account for filling and accessibility of straining sites in a manner similar to the Langmuirian blocking approach. For given values of k_{str} and β, decreasing $S_{str}^{\max}$ tends to produce higher effluent concentrations and lower values of S_{str}. The remaining

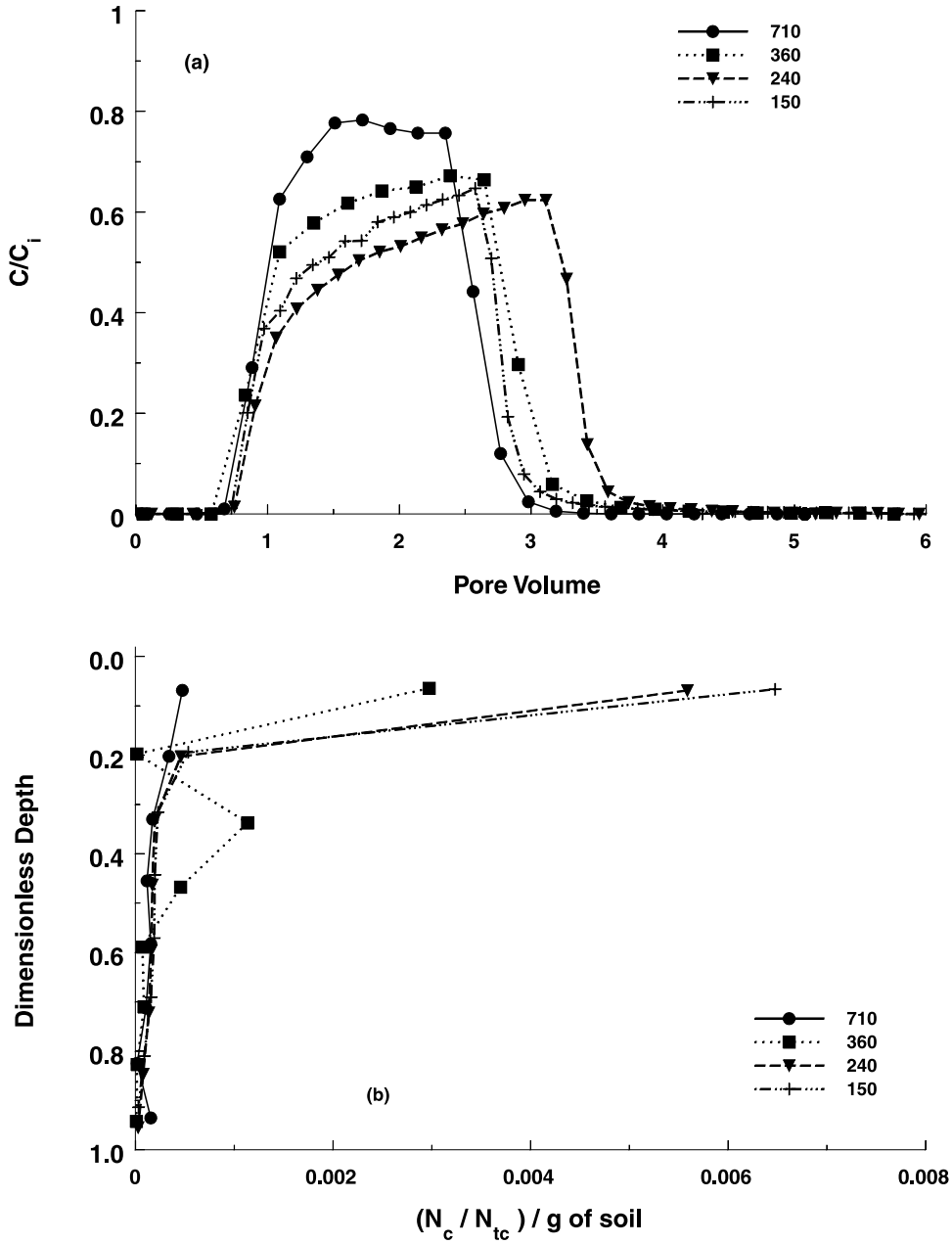

Figure 1. (a) Effluent concentration curves and (b) spatial distributions for 1.1 μm sulfate colloids in 710, 360, 240, and 150 μm sand. In Figure 1a, relative effluent concentrations (C/C_i) are plotted as a function of pore volumes, whereas in Figure 1b the normalized concentration (number of colloids, N_c, divided by the total number added to the column, N_{tc}) per gram of dry sand is plotted as a function of dimensionless distance (distance from the column inlet divided by the column length).

terms on the right-hand side of equation (4) assume that colloid mass retention by straining occurs primarily at the column inlet or textural interface because of retention of colloids in dead end pores and/or at grain junctions that are smaller than some critical size. The apparent number of dead-end pores is hypothesized to decrease with increasing distance since advection, dispersion, and size exclusion tend to keep mobile colloids within the larger networks, thus bypassing smaller pores. The potential roles of size exclusion and dispersion on colloid transport to small pores is relatively easy to understand. Water relative permeability functions for sandy soils [e.g., *van Genuchten et al.*, 1991] also suggests that water flow to the smaller regions of the pore space accounts for only a small fraction of the total permeability (saturated flow) once the flow field has been established.

[22] The HYDRUS-1D computer code [*Simunek et al.*, 1998] simulates the movement of water, heat, and multiple solutes in one-dimensional variably saturated porous media. This code was modified [*Bradford et al.*, 2003] to account for colloid attachment, detachment, straining, and blocking as outlined above. Although attachment and straining are likely to occur simultaneously in natural systems, these processes were considered separately in this work to facil-

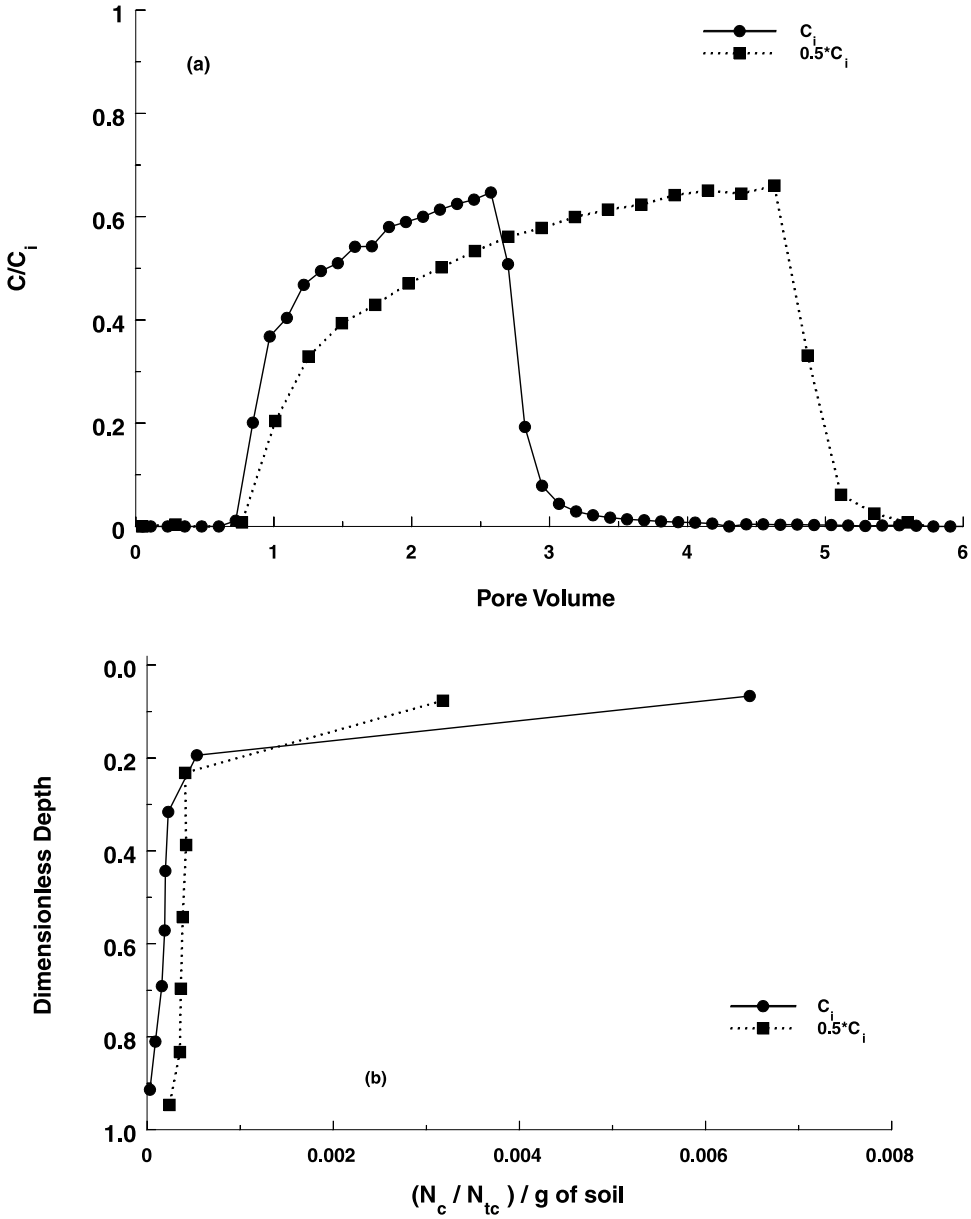

Figure 2. (a) Effluent concentration curves and (b) spatial distributions for 1.1 μm sulfate colloids in 150 μm sand at input concentrations of C_i and $0.5*C_i$.

itate the determination of unique parameter estimates for the layered systems. *Bradford et al.* [2003] and *Bradford and Bettahar* [2005] discuss several ways to estimate the magnitude of attachment and straining in homogeneous column experiments. HYDRUS-1D is coupled to a nonlinear least squares optimization routine based upon the Marquardt-Levenberg algorithm [*Marquardt*, 1963] to facilitate the estimation of solute transport parameters from experimental data.

3. Results and Discussion

3.1. Transport of 1.1 μm Colloids in Homogeneous Systems

[23] Figures 1a and 1b present effluent concentration curves and spatial distributions, respectively, for 1.1 μm sulfate colloids in 710, 360, 240, and 150 μm sands. In Figure 1a the relative effluent concentrations (C/C_i) are plotted as a function of pore volumes, whereas in Figure 1b the normalized concentration (number of colloids, N_c, divided by the total number added to the column, N_{tc}) per gram of dry sand is plotted as a function of dimensionless distance (distance from the column inlet divided by the column length). The recovered colloid mass fractions in the effluent and the sand column, as well as the total recovered mass fraction are shown in Table 1. High recovery rates were obtained using the outlined experimental materials and protocols.

[24] Figures 1a and 1b indicate that decreasing the median grain size of the sand tended to produce slightly lower effluent concentrations, and greater retention of colloids in the sand near the column inlet. Slight differences in effluent concentration curves also occurred as a result of variations in the column porosity and Darcy velocity

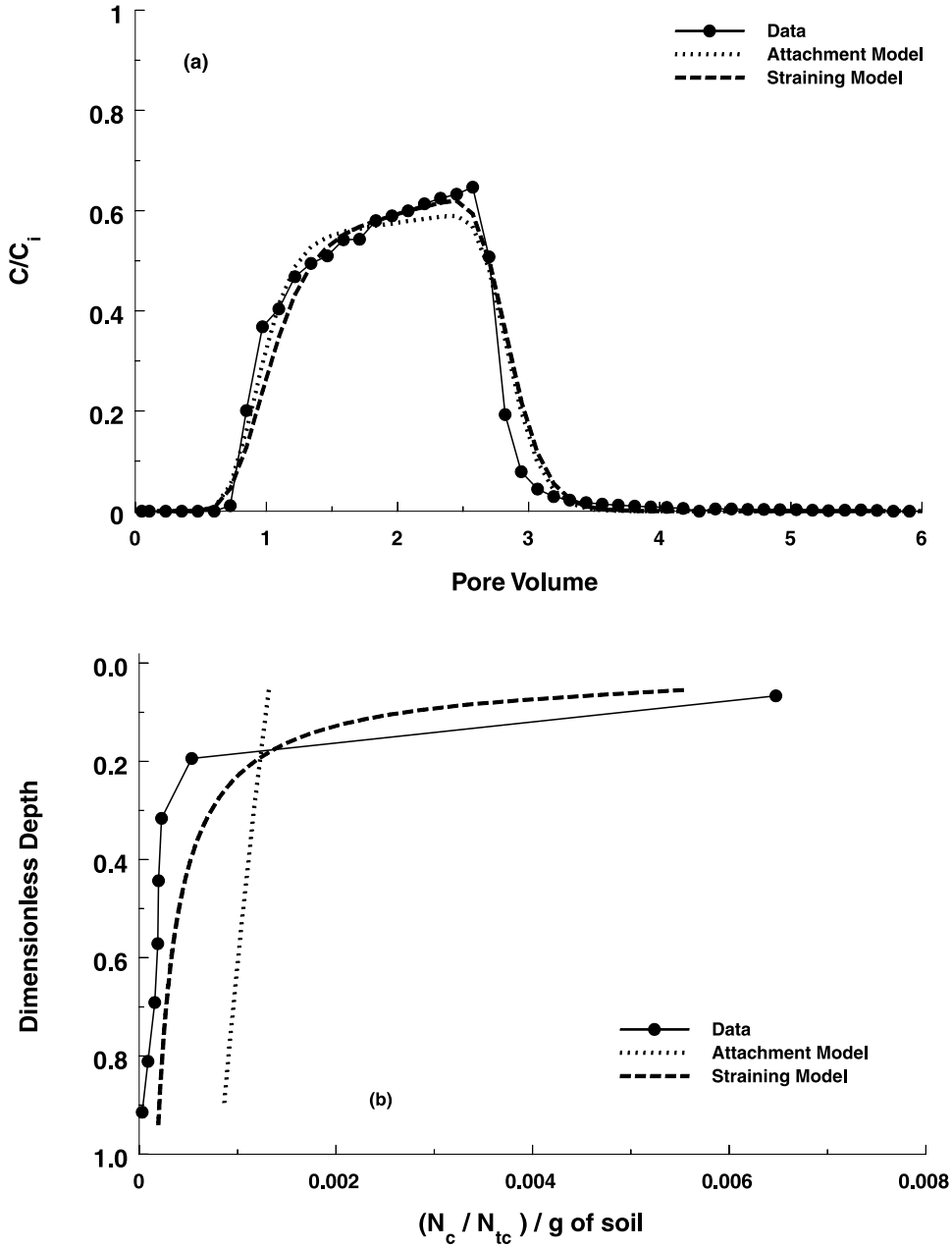

Figure 3. (a) Observed and simulated effluent concentration curves and (b) spatial distributions for 1.1 μm sulfate colloids in 150 μm sand. One of the simulations considered attachment and Langmuirian blocking (k_{det} = 0 and k_{str} = 0) according to equations (1) and (2). The other simulation considered straining (k_{att} = 0 and k_{det} = 0) according to equations (1), (3), and (4). Fitted model parameters are presented in Tables 2 and 3.

(Table 1). The transport results were consistent with the behavior of similarly sized carboxyl colloids in these same Ottawa sands as shown by *Bradford et al.* [2002]. Simulations presented by *Bradford et al.* [2003] suggests that straining was the dominant mechanism of colloid retention in these systems. Straining occurred primarily at the column inlet, presumably due to the high accessibility of potential straining sites (small pores) to flowing colloid suspensions at this location. Size exclusion and advection were hypothesized to increasingly restrict the flow of colloids to large pore networks (bypassing small, low-permeability straining sites) as the transport distance increased.

[25] After the initial colloid breakthrough, Figure 1a shows that effluent concentrations continued to slowly increase with continued colloid addition. This behavior has previously been reported in many studies [*Tan et al.*, 1994; *Liu et al.*, 1995; *Johnson and Elimelech*, 1995; *Rijnaarts et al.*, 1996; *Camesano and Logan*, 1998; *Camesano et al.*, 1999], and is referred to as blocking. Blocking implies that as favorable attachment sites become filled, attachment decreases and colloid transport is enhanced. This same explanation can also be applied to filling of straining sites. As straining sites become filled, enhanced transport occurs.

Table 2. Fitted (Hydrodynamic Dispersivity, λ_H; Attachment Coefficient, k_{att}, and Maximum Solid Phase Concentration of Attached Colloids, S_{att}^{*max}) Parameters for the Attachment (Equations (1) and (2)) Model in Homogeneous Systems (1.1 μm Colloids)[a]

Sand	d_c, μm	λ_H, cm	k_{att}, min^{-1}	S_{att}^{*max}, $N_c\,N_{tc}^{-1}$ g^{-1}	r_e^2	r_s^2
710	1.1	0.26 (0.04)	0.0047 (0.0007)	0.014 (0.023)	1.00	0.69
360	1.1	0.49 (0.23)	0.0110 (0.0028)	0.031 (0.117)	0.99	0.51
240	1.1	0.20 (0.15)	0.0231 (0.0042)	0.004 (0.004)	0.99	0.43
150	1.1	0.28 (0.18)	0.0156 (0.0011)	0.005 (0.003)	0.98	0.40
150[b]	1.1	0.28	0.0246 (0.0051)	0.003 (0.002)	0.92	0.42

[a]Standard error values for the parameter fits are provided within the parentheses.
[b]Input concentration equal to 0.5*C_i. The value of λ_H was taken from the C_i experiment.

[26] The rate of filling of straining sites was anticipated to depend on the concentration of colloids in suspension [*Foppen et al.*, 2005]. To further examine this hypothesis, an additional transport experiment was conducted at an input concentration of 0.5*C_i. Figure 2 presents effluent concentration curves (Figure 2a) and spatial distributions (Figure 2b) for 1.1 μm sulfate colloids in 150 μm sand at input concentrations of C_i and 0.5*C_i. Notice that the effluent concentration curve for the 0.5*C_i system exhibits a more gradual increase in relative concentration than the C_i system. Similar relative effluent concentrations occurred, however, after adding equal colloid masses (twice the number of pore volumes for 0.5 C_i than C_i systems). Slight differences were also observed between the C_i and 0.5*C_i spatial distributions. The 0.5*C_i system exhibited slightly lower retained concentrations near the column inlet then the C_i system, while further in the column (dimensionless distance > 0.25) this trend was reversed. These observations can be explained by the higher deposition rate that occurred in the 0.5*C_i system (it takes longer to fill the straining sites). For the colloids used in this study, the total retention capacity was independent of the input concentration (similar values of M_s in Table 1 after addition of equal colloid mass).

[27] Figures 3a and 3b present observed and simulated effluent concentration curves and spatial distributions, respectively, for 1.1 μm sulfate colloids in 150 μm sand. One of the simulations (dotted line) considered attachment and Langmuirian blocking (k_{det} and k_{str} were set equal to zero) according to equations (1) and (2). Table 2 presents attachment and blocking model parameters (hydrodynamic dispersivity, λ_H; attachment coefficient, k_{att}; and maximum solid phase concentration of attached colloids, $S_{att}^{*max} = S_{att}^{max}/N_{tc}$) that were fitted to the transport data for the various homogeneous systems, along with statistical parameters (SE is standard error, r_e^2 is the coefficient of linear regression for the effluent data, and r_s^2 is the coefficient of linear regression for the spatial distribution data) reflecting the goodness of fit. The other simulation in Figure 3 considered only straining (k_{det} and k_{att} terms were set equal to zero) according to equations (1), (3), and (4). Table 3 presents straining model parameters (k_{str} and $S_{str}^{*max} = S_{str}^{max}/N_{tc}$ were fitted, λ_H is the same as in Table 2, whereas β was obtained by fitting to transport data for the 150 μm system) and statistical information for the various homogeneous systems. In Figure 3 the straining model provided a much better description of the effluent and spatial distribution data than the attachment model (see r_e^2 and r_s^2 values in Tables 2 and 3). The straining model also gave improved descriptions of the colloid transport behavior for the coarser 710, 360, and 240 μm sand systems (see Tables 2 and 3). Other numerical simulations (not shown) revealed that differences in the predicted colloid migration and fate for the attachment and straining models will increase with increasing transport distance.

[28] As briefly mentioned in the introduction, various explanations for nonexponential colloid deposition have been proposed in the literature. Since the focus of this study was on colloid straining, the experimental conditions were designed to minimize the potential for colloid attachment (i.e., using uniformly sized and charged colloids, negatively charged colloids and porous media, and simple aqueous chemistry having a very low ionic strength). The mechanisms of colloid deposition were further deduced by means of a micromodel experiment. Figure 4a presents a photo of 1.1 μm colloid deposition near the micromodel chamber inlet in 150 μm sand. This photo demonstrates that many fluorescent colloids can be deposited at a given grain junction due to straining. The shape and surface roughness

Table 3. Fitted (Straining Coefficient, k_{str}, and Maximum Solid Phase Concentration of Strained Colloids, S_{str}^{*max}) and Estimated (Hydrodynamic Dispersivity, λ_H, and β) Parameters for the Straining (Equations (1), (3), and (4)) Model in Homogeneous Systems (1.1 μm Colloids)[a]

Sand	d_c, μm	λ_H, cm	β	k_{str}, min^{-1}	S_{str}^{*max}, $N_c\,N_{tc}^{-1}$ g^{-1}	r_e^2	r_s^2
710	1.1	0.264	1.31	1.065 (0.303)	0.001 (0.001)	0.99	0.65
360	1.1	0.490	1.31	2.561 (0.317)	0.020 (0.009)	0.98	0.84
240	1.1	0.203	1.31	10.99 (0.970)	0.011 (0.002)	0.98	0.97
150	1.1	0.283	1.31	13.86 (6.080)	0.014 (0.005)	0.96	0.97
150[b]	1.1	0.283	1.31	20.29 (0.001)	0.013	0.92	0.95

[a]Standard error values for the parameter fits are provided within the parentheses. Here λ_H is from Table 2; β is obtained from fitting to transport data for the 150 μm system.
[b]Input concentration equal to 0.5*C_i. The value of S_{str}^{max} was taken from the C_i experiment.

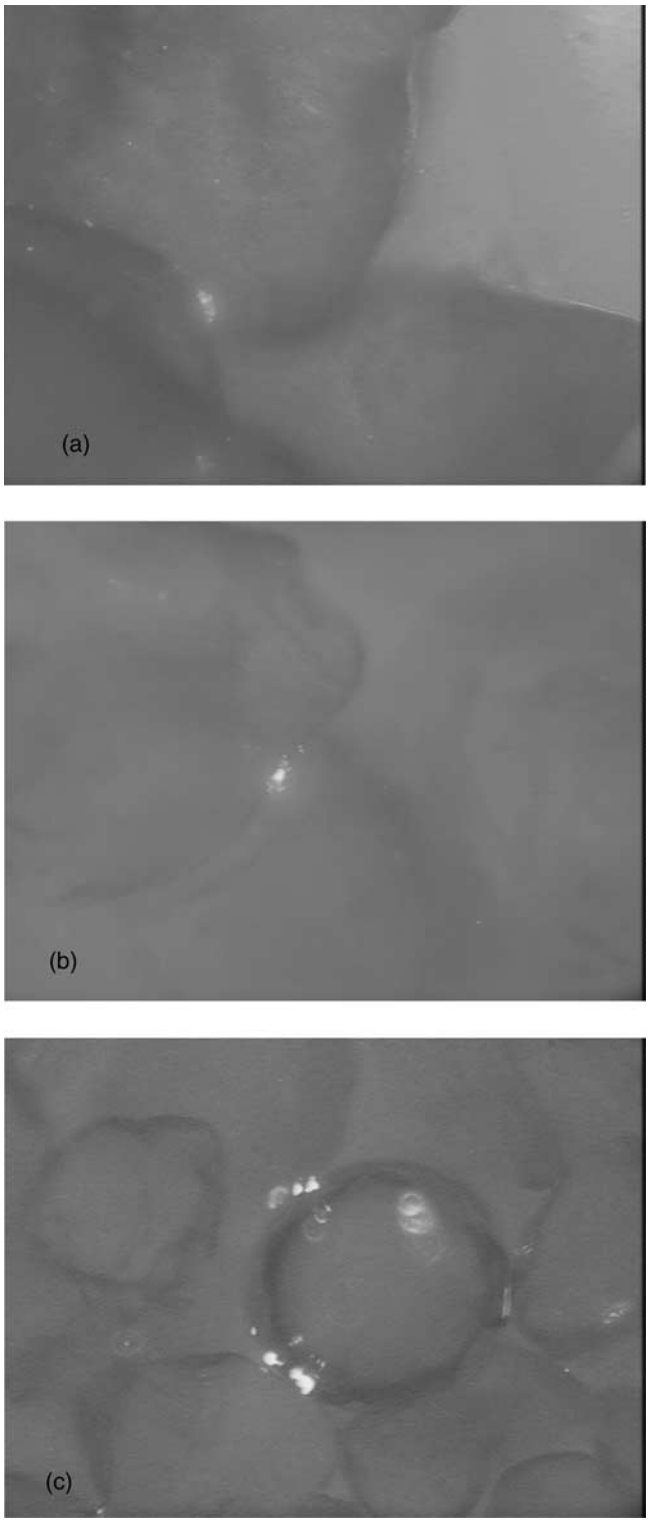

Figure 4. Photos (magnified 600 times) of colloid deposition in the micromodel experiments. (a) The 1.1 μm deposition in 150 μm sand near the chamber inlet. (b) The 1.1 μm deposition in 150 μm sand near the 710/150 textural interface. (c) The 3.0 μm deposition in 150 μm sand near the 710/150 textural interface. See color version of this figure at back of this issue.

of the sand grains are also apparent in this photo. The large number of colloids retained at this location supports our hypothesis that filling of straining sites can occur during the course of our transport experiments. Aggregation of colloids in suspension cannot explain this behavior since the uniformity of the colloid size distribution was experimentally verified with a laser scattering particle size and distribution analyzer.

3.2. Transport of 1.1 μm Colloids in Layered Systems: Fine to Coarse

[29] This section discusses the transport behavior of 1.1 μm sulfate colloids in layered sand systems when water flows from a finer-textured (150 μm sand) to a coarser-textured (710, 360, or 240 μm sand) medium. Figures 5a and 5b present relative effluent concentration curves (Figure 5a) and spatial distributions (Figure 5b) for 1.1 μm sulfate colloids in systems consisting of 150/710, 150/360, and 150/240 μm sand layers. The effluent concentration curves and spatial distributions were quite similar for the various layered systems. Decreasing the median grain size of the coarser-textured layer resulted in a slight decrease in the peak effluent concentration (Figure 5a). Figure 5b indicates that colloid retention was controlled by the finer 150 μm first layer. Little colloid retention occurred at the textural interface when flow occurs from the finer to the coarser-textured sand. Possible explanations will be discussed below.

[30] Figures 5a and 5b also show simulated effluent concentrations and spatial distributions, respectively, for the 1.1 μm sulfate colloid transport experiment (150/710, 150/360, and 150/240 μm sand layers) assuming straining (k_{det} and k_{att} were set equal to zero) in accordance with equations (1), (3), and (4). Straining model parameters, including the spatial distribution model parameter β, were taken from the corresponding homogeneous systems presented in Table 3, with the one exception of $S_{str}^{*\max}$ for the coarser-textured layer, which was fitted directly to the layered transport data (Table 4). As for the homogeneous systems, the straining model provided a good description of both the effluent (Figure 5a) and deposition (Figure 5b) data.

[31] For a given sand, the value of $S_{str}^{*\max}$ (Table 4) was always significantly smaller for the layered system than for the corresponding homogeneous system (Table 3). We hypothesize that the value of $S_{str}^{*\max}$ for the layered system should be lower because of diminished colloid accessibility to straining sites as a result of transport processes such as size exclusion, advection, and dispersion that tend to confine colloids to the hydraulically active pore network and the larger pores spaces. Similar processes were thought to occur in the homogeneous systems away from the column inlet (Figure 1b). Straining sites at the textural interfaces could also be partially filled with natural colloids that may have been mobilized during the sand cleaning process. In contrast, concentration-dependent colloid transport (Figure 2) could not account for the deposition behavior in the layered systems (Figure 5b) because of higher rates of colloid deposition at the lower input concentration (see Table 3). We will show later that straining was much more pronounced for systems involving flow from coarse to finer-textured layers.

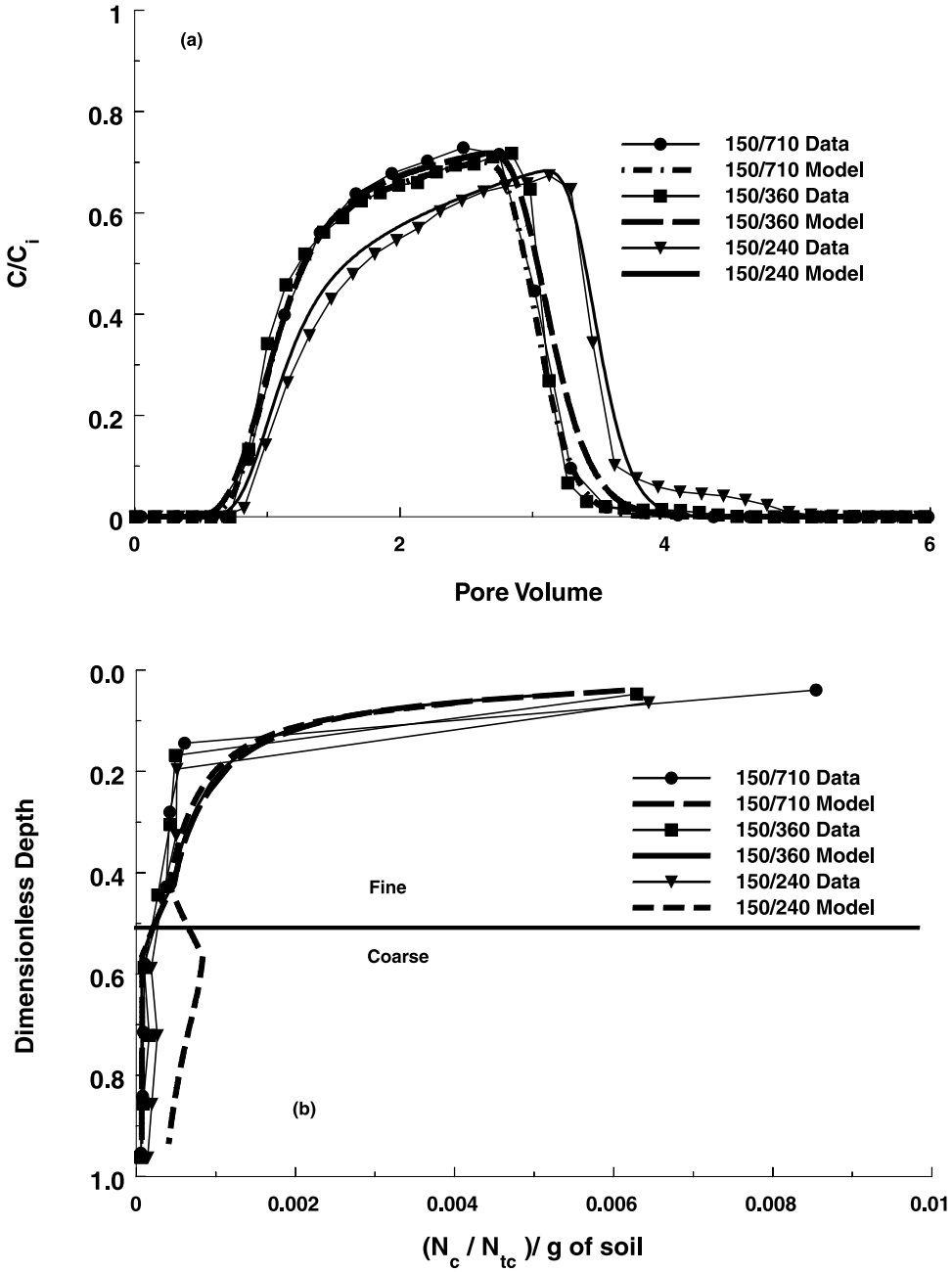

Figure 5. (a) Observed and simulated effluent concentration curves and (b) spatial distributions for 1.1 μm sulfate colloids in systems consisting of 150/710, 150/360, and 150/240 μm sand layers. Here simulations considered only straining (equations (1), (3), and (4)).

[32] When straining and attachment both occur in porous media it is difficult to separately estimate the magnitudes of these deposition processes. Colloid attachment is therefore probably best estimated in systems with little straining. Figures 5a and 5b suggest that very little straining occurred in the second layer when water flowed from a finer to a coarser-textured sand. This provides an opportunity to better estimate the magnitude of attachment in the second layer sand. For this purpose, straining was modeled only in the first layer ($k_{det} = 0$ and $k_{att} = 0$) using parameters taken from the corresponding homogeneous systems (Table 3). In the second layer only attachment was modeled ($k_{str} = 0$ and $k_{det} = 0$) by fitting a value of k_{att} to the spatial distribution data in this layer. To estimate the magnitude of k_{att} in the finest 150 μm sand, the homogeneous transport data was analyzed as a layered system (first half only straining, the second half only attachment). Simulated behavior for the finer- to coarser-textured layered systems using this approach was quite similar to that presented in Figures 5a and 5b and is therefore not shown here. The fitted values of k_{att} using this approach were 0.002, 0.002, 0.004, and 0.005 min^{-1} for the 710, 360, 240, and 150 μm sand systems, respectively. The r_s^2 values in these systems were all greater than 0.97, suggesting accurate characterization of the deposition behavior. Values of k_{att} in the homogeneous systems (Table 2) were 2.9–5.9 times greater than in these

Table 4. Fitted Values of S_{str}^{*max} (for Second Sand Layer) for the Layered Systems (1.1 μm Colloids)[a]

System	d_c, μm	S_{str}^{*max}, $N_c\ N_{tc}^{-1}$ g^{-1}	Percent S_{str}^{*max}	r_e^2	r_s^2
150/710	1.1	0.000 (0.001)	1.3	1.00	0.97
150/360	1.1	0.000 (0.000)	0.1	0.98	0.98
150/240	1.1	0.001 (0.000)	6.0	0.99	0.97
710/360	1.1	0.001 (0.000)	5.8	0.97	0.86
710/240	1.1	0.002 (0.001)	15.4	0.95	0.87
710/150	1.1	0.002 (0.000)	16.4	0.94	0.96
360/240	1.1	0.002 (0.001)	15.2	0.93	0.63
360/150	1.1	0.001 (0.000)	10.5	0.97	0.74
240/150	1.1	0.001 (0.001)	8.7	0.79	0.97

[a]The quantity "Percent S_{str}^{*max}" is used to denote the percentage of S_{str}^{*max} in the second sand layer relative to the corresponding homogeneous sand system (see Table 3). Standard error values for the parameter fits are provided within the parentheses.

"layered" systems, thus indicating that significantly less deposition occurred in the "layered" systems.

3.3. Transport of 1.1 μm Colloids in Layered Systems: Coarse to Fine

[33] This section discusses the transport behavior of 1.1 μm sulfate colloids in layered sands when water flowed from a coarser to a finer-textured medium. Figures 6a and 6b present relative effluent concentration curves (Figure 6a) and spatial distributions (Figure 6b) for 1.1 μm sulfate colloids in systems consisting of 710/360, 710/240, and 710/150 μm sand layers. Effluent concentration curves were quite similar for the various layered systems. The peak effluent concentration for the layered systems approached that of the homogeneous 710 μm sand (around 0.77). In contrast to the finer homogeneous sand systems (360, 240, and 150 μm data in Figure 1a), the effluent concentrations for the layered systems exhibited a faster rate of concentration increase with increasing colloid addition (i.e., PV). This observation suggests a more rapid filling of accessible deposition sites for the layered systems.

[34] Inspection of Figure 6b revealed similar retention of the 1.1 μm sulfate colloids in the first 710 μm layer. In contrast, the retention behavior in the second layer depended on the sand texture. The finer-textured 150 and 240 μm layers exhibited greater retention at the interface than the 360 μm layer. As for the homogeneous systems, a decrease in the median grain size of the finer-textured layer was hypothesized to produce more straining and therefore greater retention. In contrast, the layered systems exhibited significantly less retention at the textural interface than at the column inlet for the corresponding homogeneous systems (see Figure 1b). As discussed in the previous section, fewer accessible straining sites were hypothesized to exist within the layered than in homogeneous systems. This may occur as a result of transport processes (size exclusion and limited advection) as well as partial filling (deposition of natural colloids during cleaning) of straining sites at textural interfaces.

[35] An additional micromodel experiment was conducted to further support our hypothesis that straining occurred at textural interfaces. Figure 4b presents a photo of 1.1 μm colloid deposition in 150 μm sand adjacent to a 710/150 textural interface. Similar to Figure 4a, this photo demonstrates that many fluorescent colloids can be deposited at grain junctions due to straining. Very little deposition was observed in the 710 μm sand on the other side of this interface.

[36] To further illustrate the role of straining at textural interfaces, consider Figure 7, which shows relative effluent concentration curves (Figure 7a) and spatial distributions (Figure 7b) for 1.1 μm sulfate colloids in systems consisting of 710/150, 360/150, and 240/150 μm sand layers. Inspection of Figure 7 reveals a distinct trend of decreasing effluent concentration and increasing colloid retention near the column inlet with decreasing median grain size of the coarser-textured layer. These results are consistent with those for the homogeneous systems. Figure 7b indicates that colloid retention is controlled by the (first) coarser-textured layer in the 360/150 and 240/150 layered systems. Colloid retention in the 710/150 layered system, however, was dominated by the finer-textured layer due to the greater textural (permeability) contrast at this interface. Hence increasing the textural (permeability) contrast in the sand layers leads to a transition in the location of predominant straining from the column inlet to the textural interface.

[37] Figures 7a and 7b also present simulated effluent concentration curves and spatial distributions, respectively, for 1.1 μm sulfate colloids in 710/150, 360/150, and 240/150 μm sand layers. The simulations again considered straining ($k_{att} = 0$ and $k_{det} = 0$) according to equations (1), (3), and (4). The value of the S_{str}^{*max} for the (second) finer-textured layer was fitted directly to the transport data (Table 4), whereas other model parameters were obtained from the homogeneous systems (Table 3). The straining model did a reasonable job of describing both the effluent (Figure 7a) and spatial distribution (Figure 7b) data. Table 4 indicates that the value of S_{str}^{*max} increased with decreasing size of the finer-textured sand (more straining sites), and tended to increase with increasing contrast in sand texture (increased accessibility to available straining sites).

[38] The ability of the attachment model to describe colloid transport and deposition in the layered systems was also investigated. Figures 8a and 8b present observed and simulated effluent concentration curves and spatial distributions, respectively, for 1.1 μm sulfate colloids in 710/150, 360/150, and 240/150 layered systems. In this case, values of k_{att} and S_{att}^{*max} were taken from Table 2. The attachment model significantly underestimated colloid deposition at the column inlet and tended to overestimated deposition in the second layer. The simulated effluent concentrations tended to overestimate the transport potential. The values of r_e^2 and r_s^2 for the 710/150, 360/150, and 240/150 systems were 0.97 and 0.18, 0.99 and 0.11, and 0.89 and 0.47, respectively. Recall that values of k_{att} in the homogeneous systems (Table 2) were 2.9–5.9 times greater than in the finer to coarser "layered" systems. Hence utilization of k_{att} values determined in the finer to coarser "layered" systems would have predicted significantly less deposition at the column inlet and textural interface than shown in Figure 8b. Similarly, the predicted effluent concentrations would have been much higher than that shown in Figure 8a.

3.4. Transport of 3.0 μm Colloids in Homogeneous and Layered Systems

[39] This section discusses several additional experiments that were carried out with 3.0 μm sulfate colloids using both

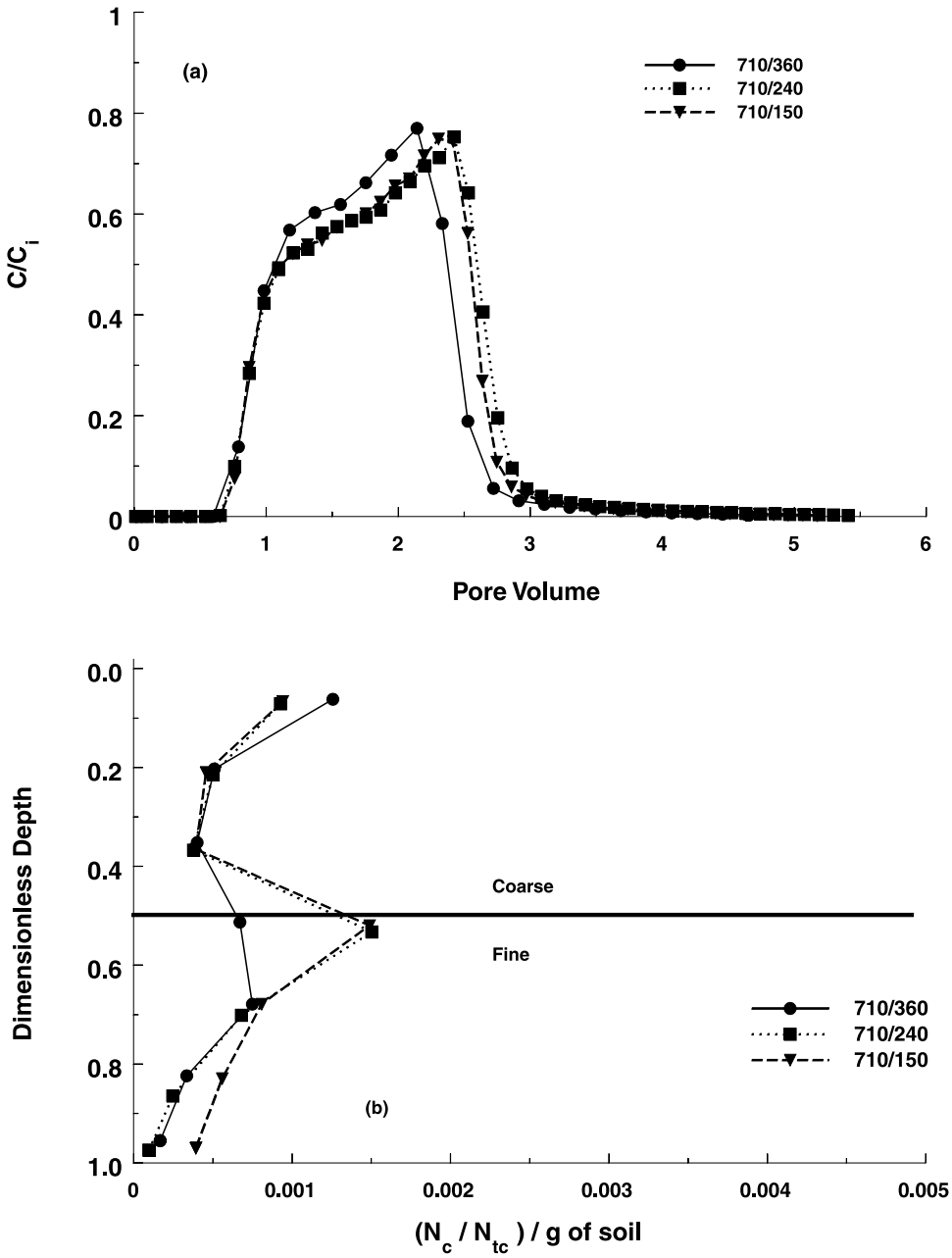

Figure 6. (a) Effluent concentration curves and (b) spatial distributions for 1.1 μm sulfate colloids in systems consisting of 710/360, 710/240, and 710/150 μm sand layers.

homogeneous (150 and 710 μm sand) and layered (150/710 and 710/150 μm sand) systems. On the basis of results by *Bradford et al.* [2002, 2003], greater straining was anticipated for 3.0 than 1.1 μm colloids in a particular sand. Transport and deposition behavior across textural interfaces was therefore expected to be more pronounced using 3.0 than 1.1 μm colloids.

[40] Figures 9a and 9b present observed effluent concentration curves and spatial distributions, respectively, for 3.0 μm colloids in systems consisting of homogeneous 150 and 710 μm sands, as well as 150/710 and 710/150 μm layered systems. As anticipated for straining behavior in the homogeneous sands, significantly more retention occurred in the 150 than the 710 μm sand. Consistent with this observation, transport and deposition in the layered systems was controlled by the 150 μm sand layer. The effluent and spatial distributions data for the layered systems, however, depended strongly on the textural order (150/710 compared to 710/150). Transport in the 150/710 layered system was similar (in terms of peak effluent concentrations, with colloid deposition occurring primarily near the column inlet) to the homogeneous 150 μm sand system. In contrast, higher effluent concentrations and significantly less deposition occurred for the 710/150 layered system compared to the homogeneous 150 μm sand or the 150/710 system. As for the

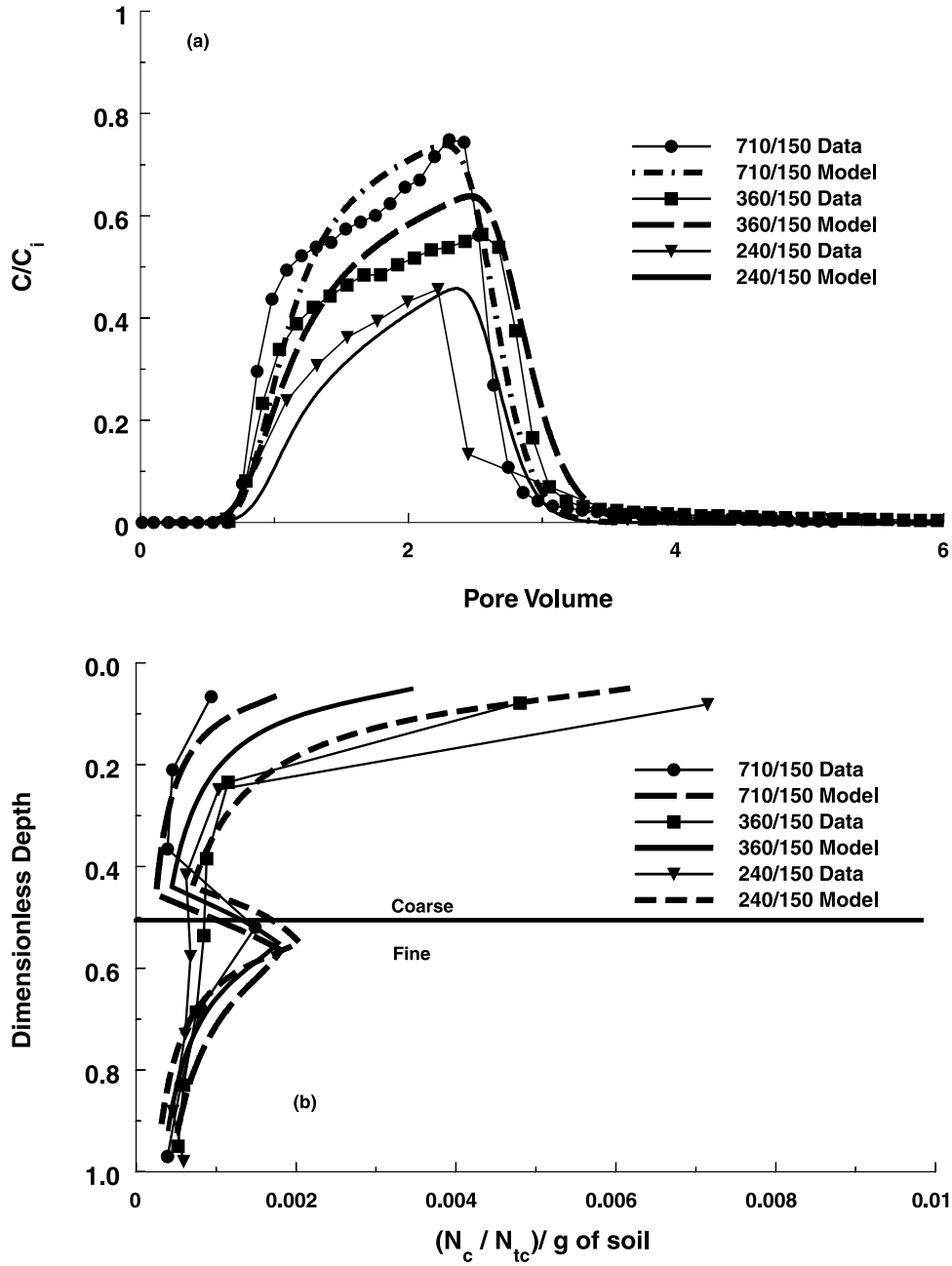

Figure 7. (a) Observed and simulated effluent concentration curves and (b) spatial distributions for 1.1 μm sulfate colloids in systems consisting of 710/150, 360/150, and 240/150 μm sand layers. Here simulations considered only straining (equations (1), (3), and (4)).

1.1 μm colloids, this behavior can be explained by transport processes (size exclusion and limited advection) or partial filling (deposition of natural colloids during cleaning) that limit accessibility of straining sites at textural interfaces. Significantly more deposition occurred at the textural interface in the 710/150 system for the 3.0 μm (Figure 9b) than the 1.1 μm (Figure 7b) colloids, suggesting increased accessibility of straining sites at textural interfaces with increasing colloid size. To further support our hypothesis that straining occurred at the 710/150 textural interface, Figure 4c presents a photo of 3.0 μm colloid deposition in 150 μm sand adjacent to a 710/150 textural interface in a micromodel experiment. Similar to Figures 4a and 4b, this photo demonstrates that fluorescent colloids can be deposited at a grain junction due to straining.

4. Summary and Conclusions

[41] Natural soil and aquifer systems frequently contain layers and lenses of contrasting soil texture. In comparison to homogeneous systems, relatively few studies have examined colloid transport and deposition at textural interfaces. Saturated packed column studies were undertaken to characterize colloid transport processes in layered sand systems. Special attention was given to the roles of colloid

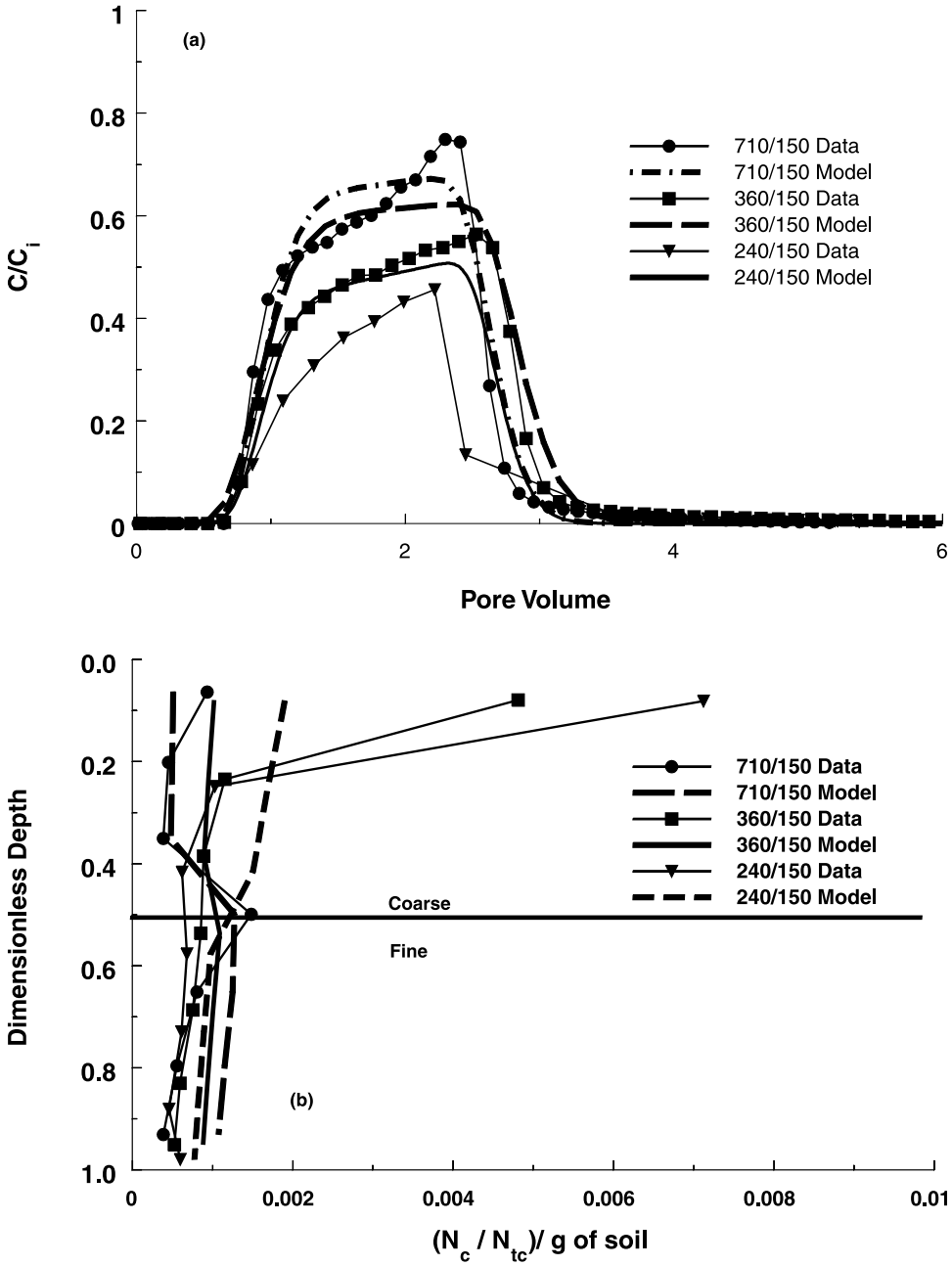

Figure 8. (a) Observed and simulated effluent concentration curves and (b) spatial distributions for 1.1 μm sulfate colloids in systems consisting of 710/150, 360/150, and 240/150 μm sand layers. Here simulations considered only attachment (equations (1) and (2)).

straining and size exclusion. Mechanisms of colloid transport and retention were deduced from measured effluent concentration curves, final spatial distributions in the columns, mass balance information, microscopic examination of deposition behavior in micromodel experiments, and numerical modeling.

[42] For a given sand and colloid, deposition was always most pronounced at the sand surface than at a textural interface. Colloids enter a new pore network at the sand surface and are therefore more likely to encounter smaller pores or dead-end regions of the pore space that contribute to straining. In contrast, we hypothesize that transport processes such as advection, dispersion and size exclusion tend to confine colloid transport to the larger pore networks at textural interfaces, and thus limit accessibility to straining sites. Increasing the textural contrast at an interface, however, produced greater colloid deposition when water flowed from coarser to finer-textured sands, suggesting an increased accessibility to straining sites in these (new) pore networks. Conversely, when water flowed from finer to coarser-textured sands, little deposition occurred. Hence colloid effluent and spatial distribution data for layered systems depended strongly on the textural order, especially for larger colloids and greater textural contrasts.

[43] Simulation of the 1.1 μm colloid transport data using a conventional attachment/detachment and blocking (Lang-

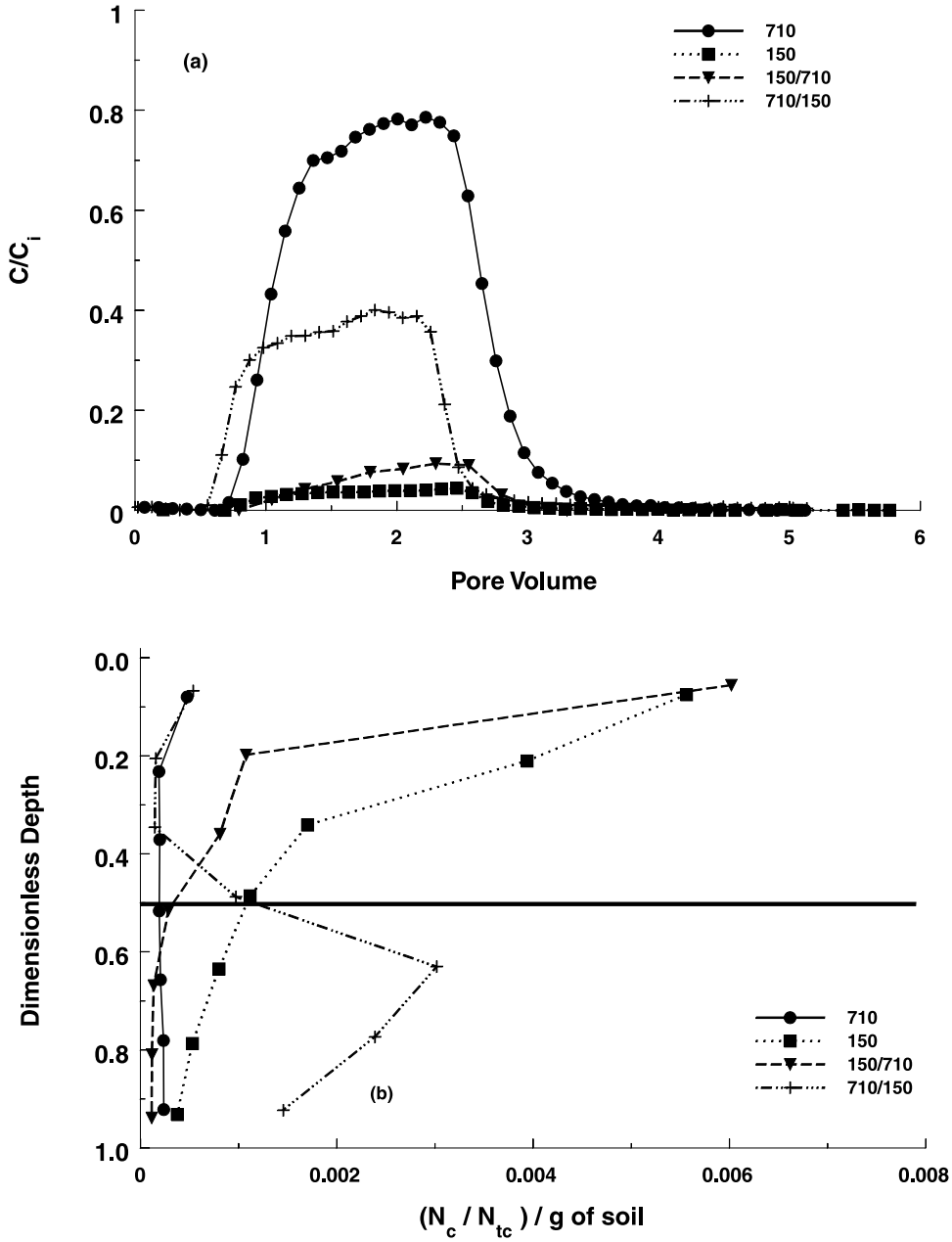

Figure 9. (a) Observed effluent concentration curves and (b) spatial distributions for 3.0 μm sulfate colloids in systems consisting of homogeneous 150 and 710 μm sands as well as 150/710 and 710/150 μm sand layers.

muirian) model provided a poor description of the spatial distribution data. A previously developed straining model was therefore modified to account for blocking (filling) and accessibility of straining sites. This model provided a satisfactory characterization of colloid effluent and spatial distribution data in both homogeneous and layered systems.

[44] Findings from this study have important implications for many colloid transport scenarios such as the design of efficient water treatment techniques based upon soil passage (riverbank filtration, infiltration basins and trenches, and sand filters), as well as the transport and fate of microorganisms and contaminants (colloid-facilitated transport) in heterogeneous systems. Knowledge of colloid transport processes across textural interfaces in unsaturated systems is, however, very limited. In this case, the topology and geometry of the hydraulically active network will greatly depend on the degree of saturation. Additional research is needed to quantify the influence of many physical (water velocity, flow bypassing, water saturation, and dimensionality), chemical (aqueous phase solution composition, surface charge of colloid and porous media), and biological factors on colloid transport and to incorporate these processes into mathematical models.

[45] **Acknowledgments.** This research was supported by the 206 Manure and Byproduct Utilization Project of the USDA-ARS. Mention of trade names and company names in this manuscript does not imply any endorsement or preferential treatment by the USDA.

References

Bitton, G., and R. W. Harvey (1992), Transport of pathogens through soil, in *New Concepts in Environmental Microbiology*, edited by R. Mitchell, pp. 103–124, John Wiley, Hoboken, N. J.

Bolster, C. H., A. L. Mills, G. M. Hornberger, and J. S. Herman (1999), Spatial distribution of bacteria experiments in intact cores, *Water Resour. Res.*, *35*, 1797–1807.

Bradford, S. A., and L. M. Abriola (2001), Dissolution of residual tetrachloroethylene in fractional wettability porous media: Incorporation of interfacial area estimates, *Water Resour. Res.*, *37*, 1183–1195.

Bradford, S. A., and M. Bettahar (2005), Straining, attachment, and detachment, of *Cryptosporidium* oocysts in saturated porous media, *J. Environ. Qual.*, *34*, 469–478.

Bradford, S. A., S. R. Yates, M. Bettahar, and J. Simunek (2002), Physical factors affecting the transport and fate of colloids in saturated porous media, *Water Resour. Res.*, *38*(12), 1327, doi:10.1029/2002WR001340.

Bradford, S. A., J. Simunek, M. Bettahar, M. T. van Genuchten, and S. R. Yates (2003), Modeling colloid attachment, straining, and exclusion in saturated porous media, *Environ. Sci. Technol.*, *37*, 2242–2250.

Bradford, S. A., M. Bettahar, J. Simunek, and M. T. Van Genuchten (2004), Straining and attachment of colloids in physically heterogeneous porous media, *Vadose Zone J.*, *3*, 384–394.

Camesano, T. A., and B. E. Logan (1998), Influence of fluid velocity and cell concentration on the transport of motile and nonmotile bacteria in porous media, *Environ. Sci. Technol.*, *32*, 1699–1709.

Camesano, T. A., K. M. Unice, and B. E. Logan (1999), Blocking and ripening of colloids in porous media and their implications for bacterial transport, *Colloids Surf. A*, *160*(3), 291–308.

Carsel, R. F., and R. S. Parrish (1988), Developing joint probability distributions of soil water retention characteristics, *Water Resour. Res.*, *24*, 755–769.

Cumbie, D. H., and L. D. McKay (1999), Influence of diameter on particle transport in a fractured shale saprolite, *J. Contam. Hydrol.*, *37*, 139–157.

Danielson, R. E., and P. L. Sutherland (1986), Porosity, in *Methods of Soil Analysis*, part 1, *Physical and Mineralogical Methods*, 2nd ed., edited by A. Klute, Soil Sci. Soc. Am., Madison, Wis.

de Jonge, L. W., C. Kjaergaard, and P. Moldrup (2004), Colloids and colloid-facilitated transport of contaminants in soils: An introduction, *Vadose Zone J.*, *3*, 321–325.

DeNovio, N. M., J. E. Saiers, and J. N. Ryan (2004), Colloid movement in unsaturated porous media: Recent advances and future directions, *Vadose Zone J.*, *3*, 338–351.

Deshpande, P. A., and D. R. Shonnard (1999), Modeling the effects of systematic variation in ionic strength on the attachment kinetics of *Pseudomonas fluorescens* UPER-1 in saturated sand columns, *Water Resour. Res.*, *35*, 1619–1627.

Elimelech, M., and C. R. O'Melia (1990), Kinetics of deposition of colloidal particles in porous media, *Environ. Sci. Technol.*, *24*, 1528–1536.

Foppen, J. W. A., A. Mporokoso, and J. F. Schijven (2005), Determining straining of *Escherichia coli* from breakthrough curves, *J. Contam. Hydrol.*, *76*, 191–210.

Ginn, T. R. (2002), A travel time approach to exclusion on transport in porous media, *Water Resour. Res.*, *38*(4), 1041, doi:10.1029/2001WR000865.

Ginn, T. R., B. D. Wood, K. E. Nelson, T. D. Schiebe, E. M. Murphy, and T. P. Clement (2002), Processes in microbial transport in the natural subsurface, *Adv. Water Res.*, *25*, 1017–1042.

Harter, T., S. Wagner, and E. R. Atwill (2000), Colloid transport and filtration of *Cryptosporidium parvum* in sandy soils and aquifer sediments, *Environ. Sci. Technol.*, *34*, 62–70.

Harvey, R. W., and H. Harms (2002), Transport of microorganisms in the terrestrial subsurface: In situ and laboratory methods, in *Manual of Environmental Microbiology*, 2nd ed., edited by C. J. Hurst et al., pp. 753–776, ASM, Washington, D. C.

Herzig, J. P., D. M. Leclerc, and P. LeGoff (1970), Flow of suspension through porous media: Application to deep filtration, *Ind. Eng. Chem.*, *62*, 129–157.

Jin, Y., and M. Flury (2002), Fate and transport of viruses in porous media, *Adv. Agron.*, *77*, 39–102.

Johnson, P. R., and M. Elimelech (1995), Dynamics of colloid deposition in porous media: Blocking based on random sequential adsorption, *Langmuir*, *11*, 801–812.

Kretzschmar, R., K. Barmettler, D. Grolimund, Y.-D. Yan, M. Borkovec, and H. Sticher (1997), Experimental determination of colloid deposition rates and collision efficiencies in natural porous media, *Water Resour. Res.*, *33*, 1129–1137.

Kretzschmar, R., M. Borkovec, D. Grolimund, and M. Elimelech (1999), Mobile subsurface colloids and their role in contaminant transport, *Adv. Agron.*, *66*, 121–193.

Li, X., T. D. Scheibe, and W. P. Johnson (2004), Apparent decreases in colloid deposition rate coefficients with distance of transport under unfavorable deposition conditions: A general phenomenon, *Environ. Sci. Technol.*, *38*, 5616–5625.

Liu, D., P. R. Johnson, and M. Elimelech (1995), Colloid deposition dynamics in flow-through porous media: Role of electrolyte concentration, *Environ. Sci. Technol.*, *29*, 2963–2973.

Logan, B. E., D. G. Jewett, R. G. Arnold, E. J. Bouwer, and C. R. O'Melia (1995), Clarification of clean-bed filtration models, *J. Environ. Eng.*, *121*, 869–873.

MacLeod, F. A., H. M. Lappin-Scott, and J. W. Costerton (1988), Plugging of a model rock system by using starved bacteria, *Appl. Environ. Microbiol.*, *54*, 1365–1372.

Marquardt, D. W. (1963), An algorithm for least-squares estimation of nonlinear parameters, *J. Soc. Ind. Appl. Math.*, *11*, 431–441.

Matthess, G., and A. Pekdeger (1985), Survival and transport of pathogenic bacteria and viruses in groundwater, in *Ground Water Quality*, edited by C. H. Ward, W. Giger, and P. McCarty, pp. 472–482, John Wiley, Hoboken, N. J.

McCarthy, J. F., and L. D. McKay (2004), Colloid transport in the subsurface: Past, present, and future challenges, *Vadose Zone J.*, *3*, 326–337.

McDowell-Boyer, L. M., J. R. Hunt, and N. Sitar (1986), Particle transport through porous media, *Water Resour. Res.*, *22*, 1901–1921.

Ouyang, Y., D. Shinde, R. S. Mansell, and W. Harris (1996), Colloid-enhanced transport of chemicals in subsurface environments: A review, *Crit. Rev. Environ. Sci. Technol.*, *26*, 189–204.

Redman, J. A., S. B. Grant, T. M. Olson, and M. K. Estes (2001), Pathogen filtration, heterogeneity, and the potable reuse of wastewater, *Environ. Sci. Technol.*, *35*, 1798–1805.

Redman, J. A., S. L. Walker, and M. Elimelech (2004), Bacterial adhesion and transport in porous media: Role of the secondary energy minimum, *Environ. Sci. Technol.*, *38*, 1777–1785.

Reimus, P. W. (1995), The use of synthetic colloids in tracer transport experiments in saturated rock fractures, *Rep. LA-13004-T*, Los Alamos Natl. Lab., Los Alamos, N. M.

Rijnaarts, H. H. M., W. Norde, E. J. Bouwer, J. Lyklema, and A. J. B. Zehnder (1996), Bacterial deposition in porous media related to the clean bed collision efficiency and to substratum blocking by attached cells, *Environ. Sci. Technol.*, *30*, 2869–2876.

Rockhold, M. L., R. R. Yarwood, and J. S. Selker (2004), Coupled microbial and transport processes in soils, *Vadose Zone J.*, *3*, 368–383.

Ryan, J. N., and M. Elimelech (1996), Colloid mobilization and transport in groundwater, *Colloids Surf. A*, *107*, 1–56.

Saiers, J. E., G. M. Hornberger, and C. Harvey (1994), Colloidal silica transport through structured, heterogeneous porous media, *J. Hydrol.*, *163*, 271–288.

Sakthivadivel, R. (1966), Theory and mechanism of filtration of noncolloidal fines through a porous medium, *Rep. HEL 15-5*, 110 pp., Hydraul. Eng. Lab., Univ. of Calif., Berkeley.

Sakthivadivel, R. (1969), Clogging of a granular porous medium by sediment, *Rep. HEL 15-7*, 106 pp., Hydraul. Eng. Lab., Univ. of Calif., Berkeley.

Scheibe, T. D., and B. D. Wood (2003), A particle-based model of size or anion exclusion with application to microbial transport in porous media, *Water Resour. Res.*, *39*(4), 1080, doi:10.1029/2001WR001223.

Schijven, J. F., and S. M. Hassanizadeh (2000), Removal of viruses by soil passage: Overview of modeling, processes, and parameters, *Crit. Rev. Environ. Sci. Technol.*, *30*, 49–127.

Silliman, S. E. (1995), Particle transport through two-dimensional, saturated porous media: Influence of physical structure of the medium, *J. Hydrol.*, *167*, 79–98.

Simunek, J., M. Sejna, and M. T. van Genuchten (1998), The HYDRUS-1D software package for simulating the one-dimensional movement of water, heat, and multiple solutes in variably-saturated media, version 2.0, *Rep. IGWMC-TPS-70*, 202 pp., Int. Ground Water Model. Cent., Colo. Sch. of Mines, Golden.

Sinton, L. W., M. J. Noonan, R. K. Finlay, L. Pang, and M. E. Close (2000), Transport and attenuation of bacteria and bacteriophages in an alluvial gravel aquifer, *N. Z. J. Mar. Freshwater Res.*, *34*(1), 175–186.

Tan, Y., J. T. Cannon, P. Baveye, and M. Alexander (1994), Transport of bacteria in an aquifer sand: Experiments and model simulations, *Water Resour. Res.*, *30*, 3243–3252.

Tufenkji, N., and M. Elimelech (2005), Breakdown of colloid filtration theory: Role of the secondary energy minimum and surface charge heterogeneities, *Langmuir*, *21*, 841–852.

Tufenkji, N., J. A. Redman, and M. Elimelech (2003), Interpreting deposition patterns of microbial particles in laboratory-scale column experiments, *Environ. Sci. Technol.*, *37*, 616–623.

Tufenkji, N., G. F. Miller, J. N. Ryan, R. W. Harvey, and M. Elimelech (2004), Transport of *Cryptosporidium* oocysts in porous media: Role of straining and physicochemical filtration, *Environ. Sci. Technol.*, *38*, 5932–5938.

van Genuchten, M. T., F. J. Leij, and S. R. Yates (1991), The RETC code for quantifying the hydraulic functions of unsaturated soils, *Rep. EPA 600/2-91/065*, 85 pp., U. S. Environ. Prot. Agency, Washington, D. C.

Wilson, J. T., L. E. Leach, M. Henson, and J. N. Jones (1986), In situ biorestoration as a ground water remediation technique, *Ground Water Monit. Rem.*, *6*, 56–64.

M. Bettahar, Parsons, 100 West Walnut Street, Pasadena, CA 91124, USA.

S. A. Bradford, Y. F. Tadassa, M. T. van Genuchten, and S. R. Yates, George E. Brown, Jr., Salinity Laboratory, ARS, USDA, 450 West Big Springs Road, Riverside, CA 92507-4617, USA. (sbradford@ussl.ars.usda.gov)

J. Simunek, Department of Environmental Sciences, University of California, Riverside, CA 92521, USA.

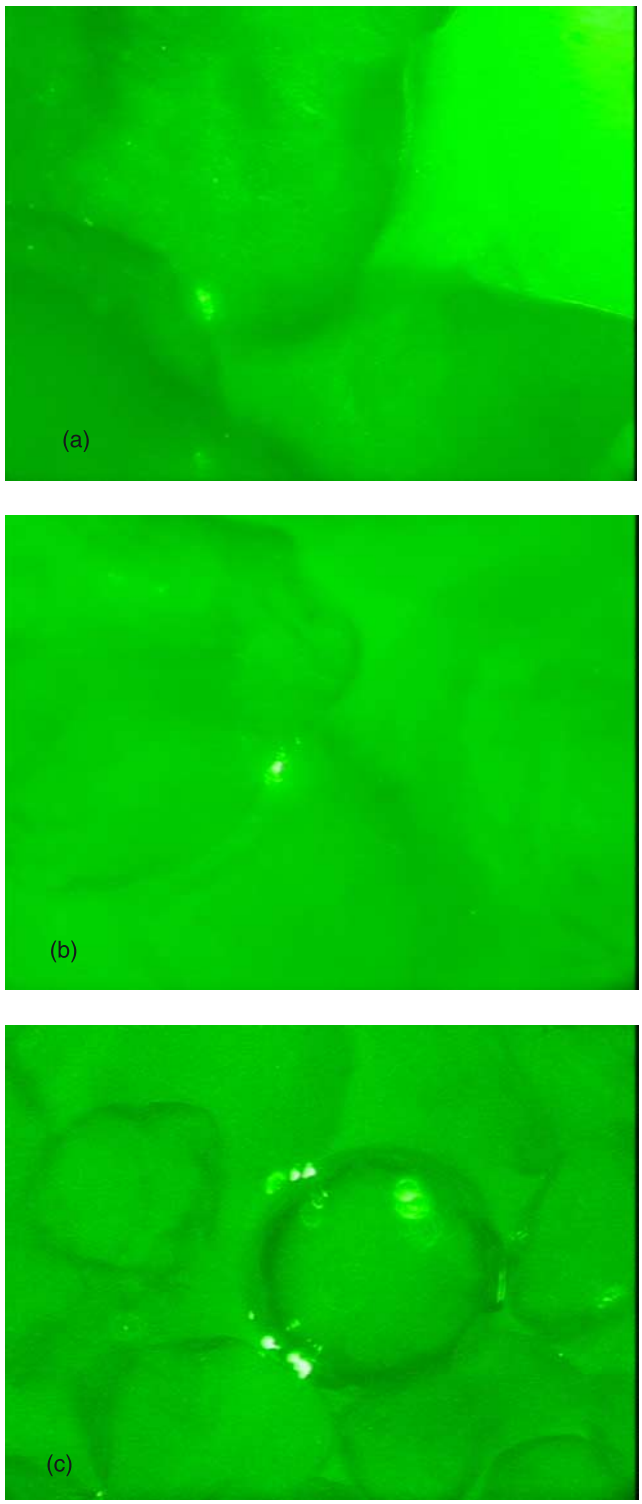

Figure 4. Photos (magnified 600 times) of colloid deposition in the micromodel experiments. (a) The 1.1 μm deposition in 150 μm sand near the chamber inlet. (b) The 1.1 μm deposition in 150 μm sand near the 710/150 textural interface. (c) The 3.0 μm deposition in 150 μm sand near the 710/150 textural interface.